Kinetics of dichotomous noise-induced transitions in a multistable multivariate system

Steve Guillouzic and Ivan L'Heureux
Ottawa-Carleton Institute for Physics, University of Ottawa, Ottawa, Ontario, Canada K1N 6N5
(Received 8 November 1996)

We study the stochastic evolution of a multivariate and deterministically multistable system subjected to an additive Markovian dichotomous noise. To this end, a steady-state probability density support is defined in such a way that no stochastic trajectory can escape. An appropriate boundary condition is then imposed in order to numerically evaluate this distribution. When the noise amplitude is large enough, the system may evolve from one deterministic attractor to another. A partition of the support in disjoint species is proposed. It is then possible to study the kinetics of the noise-induced transitions between species. Projection operator techniques are used to obtain a phenomenological kinetic law valid when the interspecies transition time scale is much longer than all the other time scales characterizing the system. We also develop a fast algorithm permitting the numerical evaluation of the phenomenological transition rate. As an example, we consider a bivariate system exhibiting two deterministic stable fixed points and a saddle point. The results confirm the existence of a phenomenological law insofar as the noise amplitude is large enough and its correlation time, small enough. [S1063-651X(97)07004-9]

PACS number(s): 02.50.Ey, 02.70.−c, 05.40.+j

I. INTRODUCTION

In nature, nonlinear dissipative systems often exhibit deterministic multistability [1–7], whereby many attractors, with their associated basins of attraction, coexist for a given set of control parameter values. Examples of such systems include many electric oscillators, chemical and photochemical reactions, optical systems, and predator-prey relationships.

All these systems are generally subjected to noise, rapid environmental fluctuations, which are usually perceived as purely random. Their action is often believed to be strictly disorganizing. It is true that the stable states of a system are blurred by the noise. However, when the noise is applied to a nonlinear system, it can create stable states with no deterministic counterpart [5,8]. As such, the noise may have a structuring effect. The influence of noise on nonlinear dissipative systems must therefore be further investigated.

White noise is often used for such investigations because of its relative ease of use. But in the case where the correlation time of the noise cannot be neglected compared to the system time scales, colored noise must be considered. The two most common types of colored noise are the Ornstein-Uhlenbeck noise and the Markovian dichotomous noise. The latter, having a discrete phase space, often leads to easier computational and experimental implementations. It is therefore a valuable tool when the influence of the noise correlation time is not negligible.

Generally, a deterministic dissipative system possesses one or more attractors. To each of them corresponds a basin of attraction. If the system is initially located in one of them, it evolves inevitably toward the corresponding attractor. When such a system is subjected to noise, a given trajectory in phase space may jump from one basin to another. These basins are not well defined anymore. As presented in Sec. II, new regions of phase space called species can be defined in analogy to chemical reactions. If the system realizations spend more time inside each of the species than to travel between them, a rate process between the different species can be defined [9]. Such transitions must not be confused with the noise-induced phase transitions described by Horsthemke and Lefever [5]. These noise-induced phase transitions occur when the stationary probability density is qualitatively modified by a change of the parameters describing the system or the noise. On the other hand, a rate process is defined for a given realization. It consists in the transition from one species to another, the parameters just mentioned being held constant.

The projection operator technique is often used in out-of-equilibrium statistical mechanics [10], for example, to study chemical reactions [11]. In recent years, it has been established that projection operator techniques are very useful for studying the evolution of the probability density in a univariate bistable system subjected to noise [9,12–15] and for investigating the transition kinetics between species in such systems, in particular for Markovian dichotomous noise. Thus, this method permitted the determination of the regime in which a phenomenological rate law properly describes the transitions between species and of an approximate analytical expression for the corresponding transition rate [9]. The memory effects that appear when a phenomenological rate law is not valid have also been investigated using projection operator techniques [9,16]. These techniques have also been used to study the critical slowing down of the interspecies transitions that occurs when the amplitude of the noise is close to the minimum value allowing those transitions to take place [9,17]. Furthermore, projection operator techniques have played a key role in the development of a numerical algorithm used to verify the validity of a phenomenological rate law and to calculate the transition rates in a univariate bistable system [17,18]. This algorithm is qualified as ''direct'' since it only considers the realizations starting at a boundary between species. On the other hand, in a simple phenomenological simulation, the realizations are initiated according to a given distribution and their evolution is monitored as a function of time. Since these transitions are very

uncommon in a regime where a phenomenological law is valid, a ''direct'' simulation is expected to be more efficient than a simple phenomenological simulation.

However, few studies have investigated the interspecies noise-induced transitions in dissipative systems described by more than one variable [19]. In this paper, we propose such a generalization of the direct simulation algorithm to multivariate multistable systems. In order to do so, we numerically determine the support over which the steady-state probability density is nonzero as well as the steady-state probability density. We also need to establish an appropriate definition for the species.

In Sec. II, we derive the general analytical expressions underlying the method. The next two sections present the numerical results for a simple example of a bivariate bistable system. Section III discusses the steady-state probability densities while Sec. IV presents the transition rates in the regime where a phenomenological law is valid. Finally, concluding remarks are found in Sec. V. Two Appendixes complete the presentation.

II. FORMALISM

A. Steady-state probability densities

We consider a system described by an n-components vector $\vec{x}$ whose evolution equation is

$$\dot{\vec{x}}=\vec{F}(\vec{x})+\vec{I}(t), \tag{2.1}$$

where $\vec{F}(\vec{x})$ is a pseudoforce and $\vec{I}(t)$ is an additive symmetric Markovian dichotomous noise sampled according to a Poisson distribution. It is characterized by [5,20–22]

$$\vec{I}(t)\in\{-\vec{\Delta},+\vec{\Delta}\},$$

$$\langle\vec{I}(t)\rangle=0,$$

$$\langle\vec{I}(t)\cdot\vec{I}(t+\tau)\rangle=|\vec{\Delta}|^2\ \exp(-\gamma|\tau|),$$

where $\gamma=2/\tau_{\rm cor}$, $\tau_{\rm cor}$ being the noise correlation time, $\vec{\Delta}$ is the noise amplitude, and $\langle\cdots\rangle$ denotes an average over realizations.

Let $p_{\pm}(\vec{x},t)d^nx$ be the probability that the system be in state $\vec{x}$ at time t with the noise being $\pm\vec{\Delta}$. It can be shown [5] that the evolution of the probability densities $p_{\pm}(\vec{x},t)$ is given by

$$\frac{\partial\mathbf{p}}{\partial t}(\vec{x},t)=\mathbf{D}\mathbf{p}(\vec{x},t), \tag{2.2}$$

where

$$\mathbf{p}(\vec{x},t)=\begin{bmatrix}p_+(\vec{x},t)\\ p_-(\vec{x},t)\end{bmatrix},$$

$$\mathbf{D}=\begin{bmatrix}-\vec{\nabla}\cdot[\vec{F}(\vec{x})+\vec{\Delta}]-\gamma/2 & \gamma/2\\ \gamma/2 & -\vec{\nabla}\cdot[\vec{F}(\vec{x})-\vec{\Delta}]-\gamma/2\end{bmatrix}.$$

We define the probability density $P(\vec{x},t,)$ projected onto the dynamical variables and the difference $Q(\vec{x},t)$ between the densities $p_{\pm}(\vec{x},t)$ as

$$P(\vec{x},t)\equiv p_+(\vec{x},t)+p_-(\vec{x},t),$$

$$Q(\vec{x},t)\equiv p_+(\vec{x},t)-p_-(\vec{x},t), \tag{2.3}$$

as well as the vector fields

$$\vec{J}(\vec{x},t)\equiv\vec{F}(\vec{x})P(\vec{x},t)+\vec{\Delta}Q(\vec{x},t),$$

$$\vec{K}(\vec{x},t)\equiv\vec{F}(\vec{x})Q(\vec{x},t)+\vec{\Delta}P(\vec{x},t). \tag{2.4}$$

Equation (2.2) then becomes

$$\frac{\partial P}{\partial t}(\vec{x},t)=-\vec{\nabla}\cdot\vec{J}(\vec{x},t),$$

$$\frac{\partial Q}{\partial t}(\vec{x},t)=-\vec{\nabla}\cdot\vec{K}(\vec{x},t)-\gamma Q(\vec{x},t). \tag{2.5}$$

It is clear that $\vec{J}(\vec{x},t)$ represents the current density associated with the probability density $P(\vec{x},t)$. Using Eqs. (2.1) and (2.3), Eq. (2.4) can be rewritten as

$$\vec{J}(\vec{x},t)=\dot{\vec{x}}_+(\vec{x})p_+(\vec{x},t)+\dot{\vec{x}}_-(\vec{x})p_-(\vec{x},t),$$

$$\vec{K}(\vec{x},t)=\dot{\vec{x}}_+(\vec{x})p_+(\vec{x},t)-\dot{\vec{x}}_-(\vec{x})p_-(\vec{x},t).$$

It now appears that $\vec{J}(\vec{x},t)$ can also be interpreted as the average velocity. On the other hand, $\vec{K}(\vec{x},t)$ characterizes the average spread of velocities in a set of realizations. As time goes to infinity, these densities and vector fields approach the steady-state distributions $p^s_{\pm}(\vec{x})$, $P^s(\vec{x})$, $Q^s(\vec{x})$, $\vec{J}^s(\vec{x})$, and $\vec{K}^s(\vec{x})$.

We consider a vector field $\vec{F}(\vec{x})$ with two or more deterministic attractors. To each of these corresponds a deterministic basin of attraction. In general, the position of the attractors and the basins extent vary randomly in time under stochastic dynamics. If the noise amplitude is large enough, a realization can therefore travel from one basin to another, thus allowing a rate process to be defined.

The steady-state probability density support (Ω) is a subregion of the phase space defined as the set of states reachable, directly or not, from any of the attractors. This definition is reasonable since every realization will eventually reach one of the attractors and subsequently all those reachable from it. The support boundary ($\partial\Omega$) is composed of segments belonging to lines defined by $\dot{\vec{x}}=\vec{F}(\vec{x})\pm\vec{\Delta}$. Therefore, everywhere on the boundary

$$\hat{N}_{\partial\Omega}\cdot[\vec{F}(\vec{x})+\vec{\Delta}]=0\quad\text{and/or}\quad\hat{N}_{\partial\Omega}\cdot[\vec{F}(\vec{x})-\vec{\Delta}]=0, \tag{2.6}$$

where $\hat{N}_{\partial\Omega}$ is a unit vector perpendicular to the boundary and pointing outside the support.

Since the system cannot be outside the support once the steady state is reached, $P^s(\vec{x})$ is zero outside it and

$$\hat{N}_{\partial\Omega}\cdot\vec{J}^s(\vec{x})=0 \tag{2.7}$$

on its boundary. Equations (2.6) and (2.7) also imply that

$$\hat{N}_{\partial\Omega}\cdot\vec{K}^s(\vec{x})=0.$$

The steady-state probability densities can be calculated using the partial differential equations (2.5) and the boundary condition (2.7):

$$\vec{\nabla}\cdot\vec{J}^s(\vec{x})=0,$$

$$\vec{\nabla}\cdot\vec{K}^s(\vec{x})+\gamma Q^s(\vec{x})=0,$$

$$\hat{N}_{\partial\Omega}\cdot\vec{J}^s(\vec{x})=0.$$

These equations cannot, in general, be solved analytically. A numerical method such as the finite elements technique is therefore required.

B. Kinetics and transition rates

Once $P^s(\vec{x})$ and $Q^s(\vec{x})$ are known, the support (Ω) can be split into m species α, to which correspond m disjoint regions Ω_α, such that $\vec{J}^s(\vec{x})$ has no component perpendicular to the boundaries $\partial\Omega_\alpha$ of these regions:

$$\hat{N}_{\partial\Omega_\alpha}\cdot\vec{J}^s(\vec{x})=0, \tag{2.8}$$

where $\hat{N}_{\partial\Omega_\alpha}$ is a unit vector perpendicular to the boundary $\partial\Omega_\alpha$ and pointing outside of the region Ω_α. The points where a vector perpendicular to the boundary cannot be defined are the only ones where a probability current density can exist between the regions Ω_α in the steady state. The species are therefore almost completely isolated from one another. This definition for the species is self-consistently determined, i.e., it springs naturally from the system characteristics instead of being arbitrarily imposed. Furthermore, it leads to a simple rate law similar to the one found in the univariate case. Finally, as will be seen from the numerical results, it leads to an *a posteriori* separation of time scales.

A characteristic function is defined for each species:

$$\theta_\alpha(\vec{x})\equiv\begin{cases}1 & \text{if} \quad \vec{x}\in\Omega_\alpha, \quad \vec{x}\notin\partial\Omega_\alpha\\ 1 & \text{if} \quad \vec{x}\in\partial\Omega_{\alpha s}\\ \frac{1}{2} & \text{if} \quad \vec{x}\in\partial\Omega_{\alpha i}\\ 0 & \text{otherwise,}\end{cases} \tag{2.9}$$

where $\partial\Omega_{\alpha i}$ is the interspecies boundary i.e., the part of $\partial\Omega_\alpha$ separating Ω_α from the other species, and $\partial\Omega_{\alpha s}$, the portion of $\partial\Omega^\alpha$ on the support's boundary excluding points belonging to $\partial\Omega_{\alpha i}$. A species average population number at time t is given by

$$\overline{N_\alpha}(t)\equiv\sum_i\int_{\Re^n}d^nx\ p_i(\vec{x},t)\,\theta_\alpha(\vec{x})$$

and its steady-state population by

$$\eta_\alpha\equiv\sum_i\int_{\Re^n}d^nx\ p_i^s(\vec{x})\,\theta_\alpha(\vec{x}),$$

where $i=\pm$. Since little probability current flows between species once the steady state is reached, we expect the average population number to vary slowly compared to the system's other degrees of freedom. We therefore define a linear operator $\mathcal{P}$ that projects onto the average population numbers in order to investigate their kinetics:

$$\mathcal{P}\rho_i(\vec{x},t)\equiv\sum_\alpha\left[\sum_j\int_{\Re^n}d^nx'\,\theta_\alpha(\vec{x}')\rho_j(\vec{x}',t)\right]\eta_\alpha^{-1}\theta_\alpha(\vec{x})p_i^s(\vec{x}), \tag{2.10}$$

where $\rho_i(\vec{x},t)$ is a function defined on the system state $\vec{x}$ and the noise $i\vec{\Delta}$. We similarly define the complementary projector $\mathcal{Q}\equiv\mathcal{I}-\mathcal{P}$, where $\mathcal{I}$ is the identity operator.

Inserting $\mathcal{P}+\mathcal{Q}=\mathcal{I}$ in the evolution equation (2.2) and projecting with $\mathcal{P}$ and $\mathcal{Q}$, we get the coupled equations:

$$\partial_t\mathcal{P}\mathbf{p}(\vec{x},t)=\mathcal{P}\mathbf{D}(\mathcal{P}+\mathcal{Q})\mathbf{p}(\vec{x},t), \tag{2.11}$$

$$\partial_t\mathcal{Q}\mathbf{p}(\vec{x},t)=\mathcal{Q}\mathbf{D}(\mathcal{P}+\mathcal{Q})\mathbf{p}(\vec{x},t). \tag{2.12}$$

Integrating Eq. (2.12), and inserting the result in Eq. (2.11), we get

$$\frac{\partial}{\partial t}\mathcal{P}\mathbf{p}(\vec{x},t)=\mathcal{P}\mathbf{D}\mathcal{P}\mathbf{p}(\vec{x},t)+\mathcal{P}\mathbf{D}e^{\mathcal{Q}\mathbf{D}t}\mathcal{Q}\mathbf{p}(\vec{x},0)+\int_0^t d\sigma\ \mathcal{P}\mathbf{D}e^{\mathcal{Q}\mathbf{D}\sigma}\mathcal{Q}\mathbf{D}\mathcal{P}\mathbf{p}(\vec{x},t-\sigma). \tag{2.13}$$

Let τ_{pop} be the time scale associated to the population dynamics and τ_{mic} the next largest time scale in the system. We assume a good separation of time scales ($\tau_{\text{pop}}\gg\tau_{\text{mic}}$). In that case, the initial condition term in Eq. (2.13) decreases rapidly. It can therefore be neglected for $t\gg\tau_{\text{mic}}$. Alternatively, it can be shown that $\mathcal{Q}\mathbf{p}(\vec{x},0)=0$ if $\mathbf{p}(\vec{x},0)$ is proportional to $\mathbf{p}^s(\vec{x})$ separately in each region. Since when $\tau_{\text{pop}}\gg\tau_{\text{mic}}$, $\mathbf{p}(\vec{x},t)$ approaches rapidly such a distribution, it is reasonable to neglect such a term.

Substituting $\mathcal{P}$'s definition, integrating over an arbitrary region Ω_β (associated with the species β) and summing over the noise, we get an equation describing explicitly the population kinetics:

$$\dot{\overline{N}}_\beta(t)=\sum_{ij\alpha}\int_{\Re^n}d^nx\ \theta_\beta(\vec{x})\mathcal{P}D_{ij}p_j^s(\vec{x})\,\theta_\alpha(\vec{x})\,\eta_\alpha^{-1}\overline{N_\alpha}(t)+\int_0^t d\sigma\sum_{ijkl\alpha}\int_{\Re^n}d^nx\ \theta_\beta(\vec{x})\mathcal{P}D_{ij}(e^{\mathcal{Q}\mathbf{D}\sigma})_{jk}\times\mathcal{Q}D_{kl}p_l^s(\vec{x})\,\theta_\alpha(\vec{x})\,\eta_\alpha^{-1}\overline{N_\alpha}(t-\sigma). \tag{2.14}$$

Using the fact that $\Sigma_\alpha\theta_\alpha(\vec{x})=1$ on all the support and also $\mathbf{D}\mathbf{p}^s(\vec{x})=0$, Eq. (2.14) can be formulated in terms of the deviations from the steady-state populations $\delta N_\alpha(t)\equiv\overline{N_\alpha}(t)-\eta_\alpha$:

$$\delta\dot{N}_\beta(t)=\sum_{ij\alpha}\int_{\Re^n}d^nx\ \theta_\beta(\vec{x})\mathcal{P}D_{ij}p_j^s(\vec{x})\,\theta_\alpha(\vec{x})\,\eta_\alpha^{-1}\delta N_\alpha(t)$$
$$+\int_0^t d\sigma\sum_{ijkl\alpha}\int_{\Re^n}d^nx\ \theta_\beta(\vec{x})\mathcal{P}D_{ij}(e^{\mathcal{Q}\mathbf{D}\sigma})_{jk}$$
$$\times\mathcal{Q}D_{kl}p_l^s(\vec{x})\,\theta_\alpha(\vec{x})\,\eta_\alpha^{-1}\delta N_\alpha(t-\sigma).$$

Since $\Sigma_i\int_{\Re^n}d^nx\ \theta_\beta(\vec{x})\mathcal{P}\rho_i(\vec{x},t)=\Sigma_j\int_{\Re^n}d^nx'\,\theta_\beta(\vec{x'})\rho_j(\vec{x'},t)$, we can eliminate $\mathcal{P}$ from the preceding equation. It becomes

$$\delta\dot{N}_\beta(t)=\delta\dot{N}'_\beta(t)+\delta\dot{N}''_\beta(t),\tag{2.15}$$

where

$$\delta\dot{N}'_\beta(t)\equiv\sum_{ij\alpha}\int_{\Re^n}d^nx\ \theta_\beta(\vec{x})D_{ij}[p_j^s(\vec{x})\,\theta_\alpha(\vec{x})]\,\eta_\alpha^{-1}\delta N_\alpha(t),$$

$$\delta\dot{N}''_\beta(t)\equiv\int_0^t d\sigma\sum_{ijkl\alpha}\int_{\Re^n}d^nx\ \theta_\beta(\vec{x})D_{ij}[(e^{\mathcal{Q}\mathbf{D}\sigma})_{jk}$$
$$\times\mathcal{Q}D_{kl}p_l^s(\vec{x})\,\theta_\alpha(\vec{x})]\,\eta_\alpha^{-1}\delta N_\alpha(t-\sigma).$$

Again using $\mathbf{D}\mathbf{p}^s(\vec{x})=0$, we get

$$\delta\dot{N}'_\beta(t)=-\sum_\alpha\ \eta_\alpha^{-1}\delta N_\alpha(t)\int_{\Re^n}d^nx\ \theta_\beta(\vec{x})\vec{J}^s(\vec{x})\cdot\vec{\nabla}\,\theta_\alpha(\vec{x}).$$

As shown in Appendix A, the characteristic function's gradient corresponds to a Dirac delta function giving us the component of a vector perpendicular to the boundary. As such,

$$\delta\dot{N}'_\beta(t)=\sum_\alpha\ \eta_\alpha^{-1}\delta N_\alpha(t)\int_{\partial\Omega_\alpha}d^{n-1}x\ g(\vec{x})\,\theta_\beta(\vec{x})$$
$$\times\hat{N}_{\partial\Omega_\alpha}\cdot\vec{J}^s(\vec{x}),$$

where the procedure of integration and the function $g(\vec{x})$ are defined in Appendix A. Since by definition $\hat{N}_{\partial\Omega_\alpha}\cdot\vec{J}^s(\vec{x})=0$, then $\delta\dot{N}'_\beta(t)=0$. The instantaneous flux therefore plays no role in the population dynamics. Memory effects are the key factor. Similarly, it can be shown that $\mathcal{P}D_{kl}p_l^s(\vec{x})\,\theta_\alpha(\vec{x})=0$. We can therefore rewrite Eq. (2.15) as

$$\delta\dot{N}_\beta(t)=-\sum_\alpha\int_0^t d\sigma\ M_{\beta\alpha}(\sigma)\,\delta N_\alpha(t-\sigma),\tag{2.16}$$

where the memory function is defined as

$$M_{\beta\alpha}(t)\equiv-\sum_{ijkl}\int_{\Re^n}d^nx\ \theta_\beta(\vec{x})D_{ij}(e^{\mathcal{Q}\mathbf{D}\sigma})_{jk}$$
$$\times D_{kl}p_l^s(\vec{x})\,\theta_\alpha(\vec{x})\,\eta_\alpha^{-1}.$$

As long as the transients due to the initial state can be neglected, Eq. (2.16) is formally exact.

When there is a good separation of time scales ($\tau_{\rm pop}\gg\tau_{\rm mic}$), we expect the phenomenological rate law

$$\delta\dot{N}_\beta(t)=-\sum_\alpha\ \tau_{\beta\alpha}^{-1}\delta N_\alpha(t)\tag{2.17}$$

to describe properly the population number kinetics. Here, the coefficients $\tau_{\beta\alpha}^{-1}$ may be positive or negative and their absolute values represent the phenomenological rate coefficients. In order for this to be the case, $M_{\beta\alpha}(t)$ must approach zero on a time scale on the order of $\tau_{\rm mic}$ such that $\delta N_\alpha(t)$ can be taken out of the time integral in Eq. (2.16). In that case the integrated memory function exhibits a plateau behavior for $t\gg\tau_{\rm mic}$. The transition rate $\tau_{\beta\alpha}^{-1}$ can be identified with that plateau value:

$$\tau_{\beta\alpha}^{-1}\equiv\int_0^{\Delta t}d\sigma\ M_{\beta\alpha}(\sigma),$$

where $\Delta t\gg\tau_{\rm mic}$. If we consider times short compared to the population dynamics time scale ($\Delta t\ll\tau_{\rm pop}$), the full propagator ($e^{\mathbf{D}t}$) can be substituted for the projected one ($e^{\mathcal{Q}\mathbf{D}t}$). This can be seen using the identity

$$e^{\mathcal{Q}\mathbf{D}t}=e^{\mathbf{D}t}-\int_0^t d\sigma\ e^{\mathbf{D}(t-\sigma)}\mathcal{P}\mathbf{D}e^{\mathcal{Q}\mathbf{D}\sigma}\tag{2.18}$$

and the estimate

$$\int_0^t d\sigma\ e^{\mathbf{D}(t-\sigma)}\mathcal{P}\mathbf{D}e^{\mathcal{Q}\mathbf{D}\sigma}\sim\frac{t}{\tau_{\rm pop}}\,e^{\mathbf{D}t}.\tag{2.19}$$

Indeed, in Eq. (2.19), $e^{\mathbf{D}(t-\sigma)}$ can be approximated by $e^{\mathbf{D}t}$ and taken out of the integral for $t\ll\tau_{\rm pop}$ since it operates only on slowly varying degrees of freedom. The integral then gives us a factor t and $\mathcal{P}\mathbf{D}$, a factor $\tau_{\rm pop}^{-1}$. The memory function can therefore be rewritten as

$$M_{\beta\alpha}(t)=\mathcal{M}_{\beta\alpha}(t)\left[1+\mathcal{O}\left(\frac{t}{\tau_{\rm pop}}\right)\right],$$

where

$$\mathcal{M}_{\beta\alpha}(t)\equiv-\sum_{ijkl}\int_{\Re^n}d^nx\ \theta_\beta(\vec{x})D_{ij}(e^{\mathbf{D}\sigma})_{jk}$$
$$\times D_{kl}p_l^s(\vec{x})\,\theta_\alpha(\vec{x})\,\eta_\alpha^{-1}.$$

Neglecting terms of order $\Delta t/\tau_{\rm pop}$, $\tau_{\beta\alpha}^{-1}$ can be expressed as

$$\tau_{\beta\alpha}^{-1}\simeq\mathcal{R}_{\beta\alpha}(\Delta t)\equiv\int_0^{\Delta t}d\sigma\ \mathcal{M}_{\beta\alpha}(\sigma).$$

In full ($j=\pm$):

$$\tau_{\beta\alpha}^{-1}=\frac{\eta_\alpha^{-1}}{2}\sum_{ij}\int_{\Re^n}d^nx\ \theta_\beta(\vec{x})(e^{\mathbf{D}\Delta t})_{ij}$$
$$\times[\vec{J}^s(\vec{x})+j\vec{K}^s(\vec{x})]\cdot\vec{\nabla}\,\theta_\alpha(\vec{x}),$$

where we have used the equation $\mathbf{D}\mathbf{p}^s(\vec{x})=0$. Defining the operator $\mathbf{D}^\dagger$, adjoint to $\mathbf{D}$,

$$D^{\dagger}=\begin{bmatrix}[\vec{F}(\vec{x})+\vec{\Delta}]\cdot\vec{\nabla}-\gamma/2 & \gamma/2\\ \gamma/2 & [\vec{F}(\vec{x})-\vec{\Delta}]\cdot\vec{\nabla}-\gamma/2\end{bmatrix},$$

this equation can be rewritten in the Heisenberg picture

$$\tau_{\beta\alpha}^{-1}=\frac{\eta_{\alpha}^{-1}}{2}\sum_{ij}\int_{\Re^n}d^nx[(e^{\mathbf{D}^{\dagger}\Delta t})_{ji}\theta_{\beta}(\vec{x})]\times[\vec{J}^s(\vec{x})+j\vec{K}^s(\vec{x})]\cdot\vec{\nabla}\theta_{\alpha}(\vec{x}).$$

Since $\vec{\nabla}\theta_{\alpha}(\vec{x})$ corresponds to a Dirac delta function and since $\hat{N}_{\partial\Omega_{\alpha}}\cdot\vec{J}^s(\vec{x})=0$,

$$\tau_{\beta\alpha}^{-1}=-\frac{\eta_{\alpha}^{-1}}{2}\sum_{ij}\int_{\partial\Omega_{\alpha}}d^{n-1}x\ g(\vec{x})j[(e^{\mathbf{D}^{\dagger}\Delta t})_{ji}\theta_{\beta}(\vec{x})]\times\hat{N}_{\partial\Omega_{\alpha}}\cdot\vec{K}^s(\vec{x}),$$

where the integration procedure and $g(\vec{x})$ are defined in Appendix A. As shown in Appendix B, $[\Sigma_i(e^{\mathbf{D}^{\dagger}t})_{ji}\theta_{\beta}(\vec{x})]$ represents the average over realizations at time t of the characteristic function given that at $t=0$, the system was in state $\vec{x}$ and the noise was $j\vec{\Delta}$. We define $\theta_{\beta}^r(t|\vec{x},j\vec{\Delta})$ as the value $\theta_{\beta}(\vec{x}(t))$ at time t for a given realization initiated at time $t=0$ with the system in state $\vec{x}$ and noise equal to $j\vec{\Delta}$. Thus:

$$\langle\theta_{\beta}^r(t|\vec{x},j\vec{\Delta})\rangle=\sum_i(e^{\mathbf{D}^{\dagger}t})_{ji}\theta_{\beta}(\vec{x})$$

where the average over the realizations is explicit. We now obtain the central result of this paper:

$$\tau_{\beta\alpha}^{-1}=\frac{\eta_{\alpha}^{-1}}{2}\int_{\partial\Omega_{\alpha}}d^{n-1}x\ g(\vec{x})[\langle\theta_{\beta}^r(\Delta t|\vec{x},-\vec{\Delta})\rangle-\langle\theta_{\beta}^r(\Delta t|\vec{x},+\vec{\Delta})\rangle]\hat{N}_{\partial\Omega_{\alpha}}\cdot\vec{K}^s(\vec{x}),\qquad(2.20)$$

where $\tau_{\mathrm{mic}}\ll\Delta t\ll\tau_{\mathrm{pop}}$.

For univariate systems, this equation reduces to an equation derived by L'Heureux and Kapral [17] given that we consider, like they did, only two species and use the local minimum of $P^s(\vec{x})$ as the boundary between them. The criterion $\hat{N}_{\partial\Omega}\cdot\vec{J}^s(\vec{x})=0$ cannot be used for that case since $\vec{J}^s(\vec{x})$ is identically zero.

In Eq. (2.20), the component of $\vec{K}^s(\vec{x})$ perpendicular to $\partial\Omega_{\alpha}$ represents the speed at which a set of realizations splits apart perpendicularly to the boundary. Also, the difference between the averaged characteristic functions then represents the evolution of the realizations after they have left the boundary, indicating the fraction of realizations that end up in region Ω_{β} because they are going in the right direction from the start. As in the univariate case, the presence or the absence of a plateau for $\mathcal{R}_{\beta\alpha}(\Delta t)$ ($\tau_{\mathrm{mic}}\ll\Delta t\ll\tau_{\mathrm{pop}}$) constitutes a validity criterion for the phenomenological rate law (2.17).

This law can be rewritten as $\delta\dot{\mathbf{N}}(t)=-\mathbf{K}\delta\mathbf{N}(t)$, where the vector $\delta\mathbf{N}(t)$ groups together the m population numbers and the matrix $\mathbf{K}$, the m^2 transition coefficients $\tau_{\beta\alpha}^{-1}$. The normalization condition $\Sigma_{\alpha}\delta N_{\alpha}(t)=0$ implies that only m^2-m transition rates are independent and that $\mathbf{K}$ is singular. The eigenvalues and eigenvectors of $\mathbf{K}$ give us some insight into the population kinetics. The null eigenvalue corresponds to the steady state. The next smallest one, named τ_{pop}^{-1}, corresponds to the largest time scale of the system. A phenomenological simulation can be used to calculate it if it is much smaller than all other nonzero transition rates. For systems with two species defined, A and B, we have

$$\tau_{\mathrm{pop}}^{-1}=\tau_{AA}^{-1}+|\tau_{AB}^{-1}|,\quad=\tau_{BB}^{-1}+|\tau_{BA}^{-1}|\qquad(2.21)$$

III. STEADY-STATE DISTRIBUTION AND SPECIES

A. Model

In this study, we concentrate on bivariate systems. In the absence of noise, the system considered here exhibits two stable fixed points and a saddle point. When subjected to dichotomous noise, its evolution is given by

$$\dot{x}=-ax^3+bx\pm\Delta_x,$$

$$\dot{y}=-cy\pm\Delta_y.$$

The amplitude of the noise is chosen in such a way that only one attractor subsists for each of its values ($\pm\vec{\Delta}$). This bivariate system is described by two deterministically decoupled subsystems, the one in x having been already studied [9,17,18]. The only coupling between the two subsystems are due to the synchronized transitions of the noise. Once numerically evaluated, the probability densities for the bivariate systems can therefore be projected on x and y and compared with the known solutions of the univariate systems.

Using reduced units

$$x=x^*\sqrt{c/a},$$

$$y=y^*\Delta_y/c,$$

$$t=t^*/c,$$

these equations can be rewritten as

$$\dot{x}^*=-(x^*)^3+b^*x^*\pm\Delta_x^*,$$

$$\dot{y}^*=-y^*\pm1,\qquad(3.1)$$

where

$$b^*=b/c$$

$$\Delta_x^*=\Delta_x\sqrt{a/c^3},$$

$$\gamma^*=\gamma/c.$$

Subsequently, we drop the asterisk while implicitly using the reduced units.

B. Algorithms

1. Determination of the support

The first step leading to the evaluation of the interspecies transition rate consists in determining the support of the steady-state probability density. As mentioned in Sec. II, it is defined as the set of all the states reachable from the attractors.

The support boundary is numerically evaluated as a sequence of segments, each of them being part of a trajectory leading toward an attractor. The computation of this sequence is a two-step process. The first one supplies an approximation to the boundary and the second iteratively improves it.

The chosen initial approximation consists of a closed curve containing no area. It is determined by a deterministic trajectory joining the two attractors. We use a starting point located at the surviving attractor when $\vec{I}(t)=+\vec{\Delta}$. The equation $\dot{\vec{x}}=\vec{F}(\vec{x})-\vec{\Delta}$ is then numerically integrated using an adaptative Runge-Kutta algorithm in order to get a sequence of points on a deterministic trajectory joining the two attractors. Using these points, a closed and degenerate loop encompassing no area is built. This sequence of points constitutes the initial approximation of the support boundary. A different but equally valid approximation is obtained if the attractor surviving when $\vec{I}(t)=-\vec{\Delta}$ is chosen as the starting point and if the equation $\dot{\vec{x}}=\vec{F}(\vec{x})+\vec{\Delta}$ is numerically integrated.

As mentioned above, the second step consists of a loop where the approximation is refined until sufficient precision is attained. It is important to note that the initial approximation is a subset of the support as is every subsequent approximation. We therefore iteratively extend the support until convergence is obtained. To do this, we consider successively each of the points that define the segments approximating the support. For each point, we verify if there exists a deterministic trajectory, described by $\dot{\vec{x}}=\vec{F}(\vec{x})-\vec{\Delta}$ or $\dot{\vec{x}}=\vec{F}(\vec{x})+\vec{\Delta}$, going through it and leading outside the support as described by the current approximation. If this is the case, we numerically integrate the corresponding equation until the deterministic trajectory reaches the current support approximation. The latter is then updated to include the region just calculated. In doing so, we eliminate the part of the boundary that is not on the support boundary anymore. We then continue to examine each point one at a time, but considering only those that define the new approximation of the support boundary. When no deterministic trajectory lead outside of the support, we consider that it has been entirely determined.

Even if it may seem complicated, this procedure is very efficient. Only a few minutes are required to determine the support for a given problem on an average workstation. However, the algorithm performance is tied to the order in which we use the trajectories that lead outside the support approximation. It is clearly advantageous to first use those that increase the size of the approximation by the greatest amount since it minimizes the number of iterations.

2. Finite elements

The support being determined, the steady-state probability density is then numerically evaluated using a finite elements algorithm [23]. This method was chosen over the finite difference algorithm because of the relative ease with which it considers boundaries of arbitrary shape. The finite elements algorithm has been implemented using the Modulef library developed by the Institut National de Recherche en Informatique et en Automatique (France).

We consider the following two partial differential equations and the corresponding boundary condition:

$$\vec{\nabla}\cdot\vec{J}^{s}(\vec{x})=0, \tag{3.2}$$

$$\vec{\nabla}\cdot\vec{K}^{s}(\vec{x})+\gamma Q^{s}(\vec{x})=0, \tag{3.3}$$

$$\hat{N}_{\partial\Omega}\cdot\vec{J}^{s}(\vec{x})=0, \tag{3.4}$$

where $\hat{N}_{\partial\Omega}$ is a unit vector normal to the boundary and pointing outside the support. As was seen in Sec. II, Eq. (3.4) also implies

$$\hat{N}_{\partial\Omega}\cdot\vec{K}^{s}(\vec{x})=0. \tag{3.5}$$

As is well known, the finite elements method consists in using a mesh and interpolation functions to transform the partial differential equations to a system of linear equations. The starting point of the finite elements method consists in multiplying Eqs. (3.2) and (3.3) by the arbitrary functions $H_J(\vec{x})$ and $H_K(\vec{x})$ and in integrating them over the support:

$$\int_{\Omega} d^2x\ H_J(\vec{x})\vec{\nabla}\cdot\vec{J}^{s}(\vec{x})=0,$$

$$\int_{\Omega} d^2x\ H_K(\vec{x})[\vec{\nabla}\cdot\vec{K}^{s}(\vec{x})+\gamma Q^{s}(\vec{x})]=0.$$

Using the divergence theorem and the boundary conditions (3.4) and (3.5), we obtain the so-called weak formulation:

$$\int_{\Omega} d^2x\vec{\nabla}H_J(\vec{x})\cdot\vec{J}^{s}(\vec{x})=0,$$

$$\int_{\Omega} d^2x[\vec{\nabla}H_K(\vec{x})\cdot\vec{K}^{s}(\vec{x})-\gamma H_K(\vec{x})Q^{s}(\vec{x})]=0.$$

It implicitly contains the boundary conditions. They are therefore natural boundary conditions and do not need to be forced when the linear system of equations is solved. The last step in preparing the partial differential equations is to substitute the definitions of $\vec{J}^{s}(\vec{x})$, $\vec{K}^{s}(\vec{x})$, and $Q^{s}(\vec{x})$:

$$\int_{\Omega} d^2x(\{\vec{\nabla}H_J(\vec{x})\cdot[\vec{F}(\vec{x})-\vec{\Delta}]\}p^{s}_{-}(\vec{x})$$

$$+\{\vec{\nabla}H_J(\vec{x})\cdot[\vec{F}(\vec{x})+\vec{\Delta}]\}p^{s}_{+}(\vec{x}))=0,$$

$$\int_{\Omega} d^2x(\{-\vec{\nabla}H_K(\vec{x})\cdot[\vec{F}(\vec{x})-\vec{\Delta}]+\gamma H_K(\vec{x})\}p^{s}_{-}(\vec{x})$$

$$+\{\vec{\nabla}H_K(\vec{x})\cdot[\vec{F}(\vec{x})+\vec{\Delta}]-\gamma H_K(\vec{x})\}p^{s}_{+}(\vec{x}))=0.$$

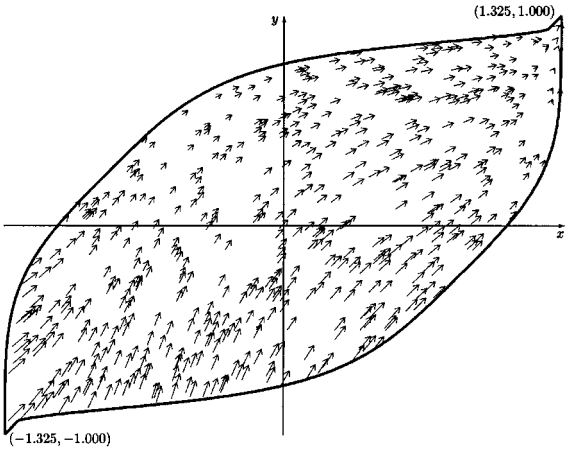

FIG. 1. Vectorial field $\vec{F}(\vec{x})+\vec{\Delta}$ for $\gamma=25$, $b=\Delta_x=1$. The arrow length is proportional to the value of the vectorial field.

These equations are then solved for $p^s_{\pm}(\vec{x})$. Since the system of linear equations is homogeneous, the solution is determined only up to a constant. The normalization condition

$$\int_{\mathfrak{R}^n} d^n x\ P(\vec{x},t)=1$$

determines that constant.

For this initial study, we chose to use the simplest possible type of finite elements, i.e., triangles with nodes at the vertices and to which are associated linear interpolation functions. The solution therefore has a continuity C^0 between elements. We use the Galerkin method, which expresses the arbitrary functions $H_J(\vec{x})$ and $H_K(\vec{x})$ in terms of the same interpolating functions as the steady-state probability densities.

3. Smoothing

The result obtained by the finite elements algorithm exhibits small amplitude oscillations superposed to the solution of the partial differential equations. These are due to the discretization procedure. In principle, their amplitude can be made as small as necessary by decreasing the size of the elements. However, limited computer resources do not allow for an infinite reduction of the element size. The most important region of phase space is the one between the peaks since this is where the interspecies boundary is located. The probability density being small in that region, it was impossible to sufficiently decrease the amplitude of these oscillations using the chosen type of finite elements.

It was therefore decided to use a smoothing procedure in order to reduce the amplitude of these undesirable oscillations. The distributions are averaged separately on each triangle using the simple formula

$$P'_{in}=P'_{jn}=P'_{kn}=\frac{P_i+P_j+P_k}{3},$$

where the variable P_m represents the initial value at global node m and P'_{mn}, the average at global node m calculated on triangle n. The averages are considered to be performed simultaneously on every triangle, i.e., the value at each node is updated only once all the averages have been calculated.

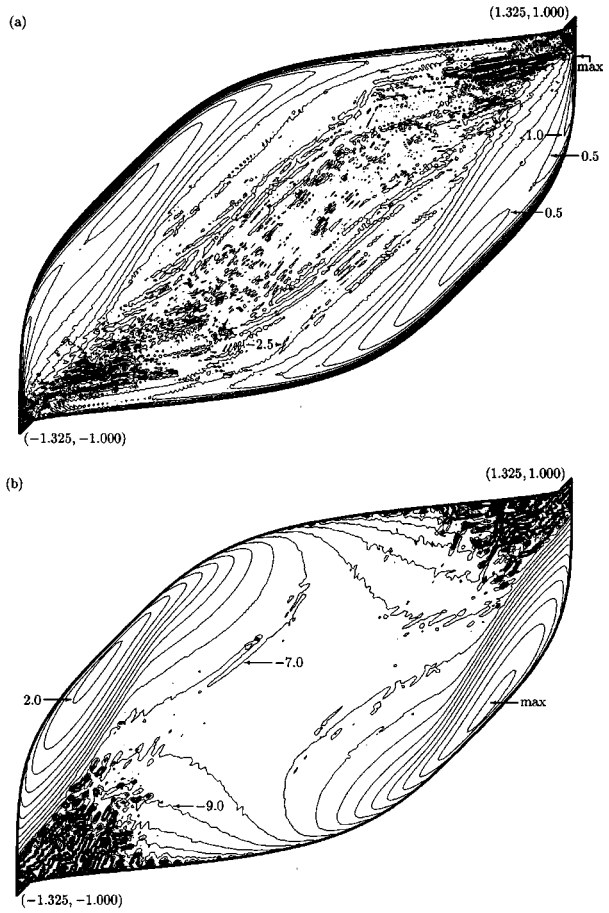

FIG. 2. $\ln P^s(\vec{x})$ for various values of γ obtained by finite elements techniques in the case where $b=\Delta_x=1$. (a) $\gamma=5$ (two smoothing cycles); the spacing between level curves is 0.5 (b) $\gamma=25$ (three smoothing cycles); the spacing between level curves is 1.0.

The last step consists in combining for each node the average value from each adjacent triangle. This in done by considering the area A_i of each triangle:

$$P''_i=\frac{\sum_j P'_{ij}A_j}{\sum_j A_j},$$

where P''_i is the new value associated with global node i. It is easily verified that the normalization is conserved.

It may be necessary to apply the smoothing more than once in order to obtain clear steady-state probability densities between the peaks for the purpose of defining a clear interspecies boundary.

4. Interspecies boundary

Once the steady-state probability densities have been evaluated, the steady-state density current $\vec{J}^s(\vec{x})$ can be computed from Eq. (2.4) and the interspecies boundary deter-

mined using criterion (2.8). The first step is to start from a point that is necessarily part of the boundary. For example, the symmetry of the problem implies that the origin is part of the interspecies boundary for the model presented in Sec. III A. From this point, we find directions tangential to the current, either upstream or downstream, and integrate all the way to the support boundary using an adaptative Runge-Kutta algorithm.

C. Results

Figure 1 shows the stochastic field $\vec{F}(\vec{x})+\vec{\Delta}$ on the support for the model presented in Sec. III A. The field $\vec{F}(\vec{x})-\vec{\Delta}$ can be obtained by a reflection through the origin. The figure illustrates the validity of the result obtained from the support determination algorithm. Since this procedure is entirely deterministic, the support shape and size do not depend on the value of γ. The presence of four vertices underlines the complexity of the behavior that can arise when a simple system is subjected to noise.

Figure 2 illustrates the steady-state probability density $P^s(\vec{x})$ and demonstrates the variety of behaviors that can arise when a simple system is subjected to Markovian dichotomous noise. The symmetry property $P^s(\vec{x})=P^s(-\vec{x})$ exhibited by the figure supports the validity of the algorithms. For γ small, the distribution in the neighborhood of the origin is small and is overwhelmed by the numerical noise. However near the edge of the support, its evaluation is reliable. It is seen that $P^s(\vec{x})$ exhibits an absolute maximum near the upper-right and lower-left corners of the support. There is also a relative maximum near the deterministic stable fixed points $(\pm 1,0)$. $P^s(\vec{x})$ is therefore quadrimodal. As γ increases, the maxima near the corners disappear, leaving a bimodal distribution. When the system is deterministically decoupled, a quantitative verification of the distribution is to project it on x and y by integrating over y and x, respectively. We can then compare the results with the known distributions for decoupled univariate systems (Fig. 3). Indeed, it has been shown [5] that for a univariate system whose evolution is described by

$$\dot{x}=F(x)+I(t),$$

where $I(t)$ is Markovian dichotomous noise, the probability density $P^s(x)$ is given by

$$P^s(x)=\begin{cases}\dfrac{Z}{D^{\mathrm{eff}}(x)}\exp[\phi(x)], & x\in[x_A,x_B]\\ 0, & x\notin[x_A,x_B],\end{cases}$$

$$\phi(x)=\int_d^x dx'\,\frac{F(x')}{D^{\mathrm{eff}}(x')}, \tag{3.6}$$

$$D^{\mathrm{eff}}(x)=\frac{\Delta^2}{\gamma}\left(1-\frac{F^2(x)}{\Delta^2}\right).$$

The constant d is arbitrary while Z is a normalization constant. The interval $[x_A,x_B]$ constitutes the support, where $x_{A,B}$ are the roots of $F(x)=\pm\Delta$, respectively.

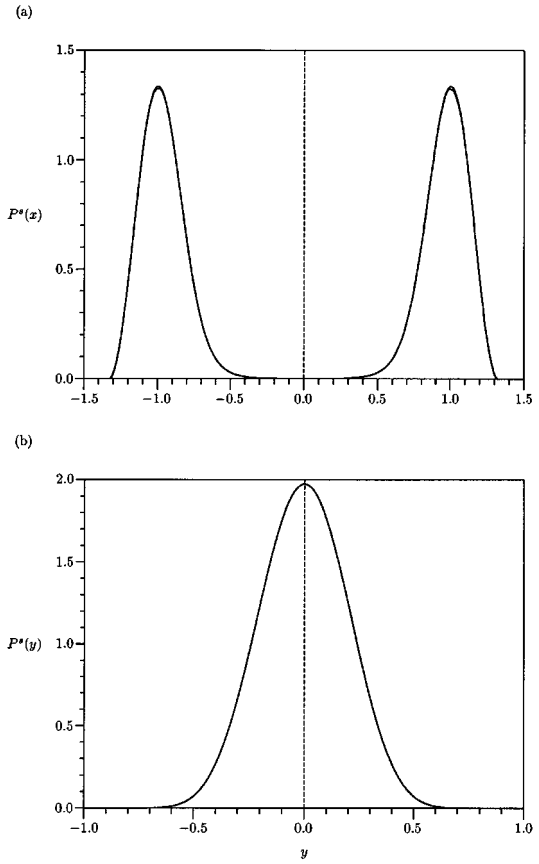

FIG. 3. Projections of $P^s(\vec{x})$ for $\gamma=25$, $b=\Delta_x=1$. The projected probability densities are practically indistinguishable from the ones calculated using Eq. (3.6). (a) Projection on x, (b) projection on y.

The probability current density is shown in Fig. 4. It is clearly seen that boundary condition (2.7) is verified. Finally, an interspecies boundary passing through the origin can be defined according to criterion (2.8) (Fig. 5). Near the origin, this boundary is close to the stable manifold of the deterministic saddle point.

IV. KINETICS

A. Algorithms

1. Phenomenological simulation

In a simple phenomenological simulation, the realizations are initiated according to some distribution and are monitored under stochastic evolution. The results can then be fitted to a phenomenological rate law. However, for regimes where such a phenomenological law is valid, the stochastic trajectories wander for a long time within each species and transitions seldom happen. Even if such a procedure can be extremely inefficient, it is used here to verify the direct simulation results.

2. Direct simulation

A different approach is suggested by Eq. (2.20), in which all trajectories start on an interspecies boundary. Since the distributions are calculated using linear interpolation functions, a simple trapezoidal algorithm is used to integrate over

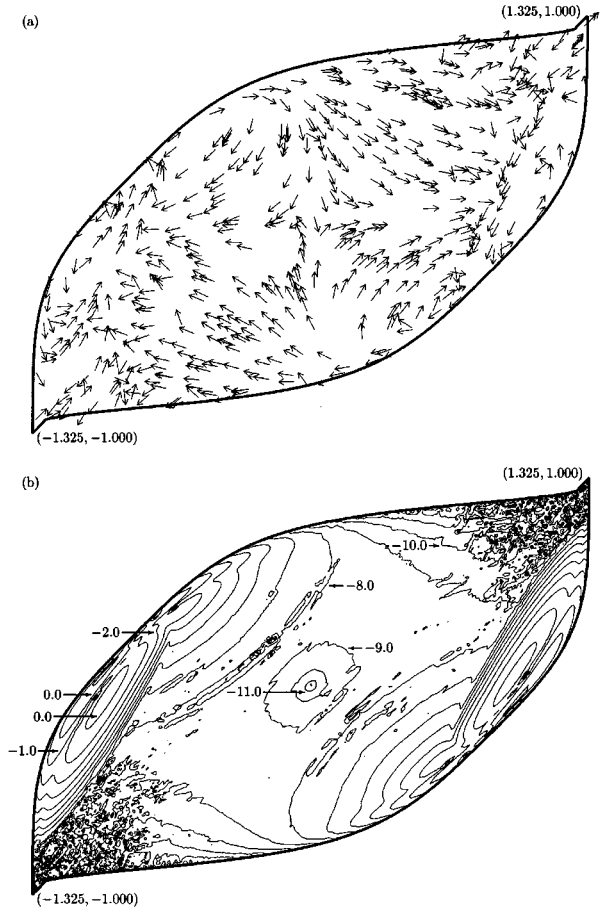

FIG. 4. Probability current density field for $\gamma=25$, $b=\Delta_x=1$. (a) $\vec{J}^s(\vec{x})/|\vec{J}^s(\vec{x})|$, (b) $\ln(|\vec{J}^s(\vec{x})|)$; the spacing between the level curves is 1.0.

the species boundary. Such an approach is expected to be much more efficient than the simple phenomenological simulation. Furthermore, using a direct simulation leads to the determination of all the transition rates that are present in a phenomenological rate law whatever the number of species may be. On the other hand, a simple phenomenological simulation can only distinguish between transition rates of different orders of magnitude.

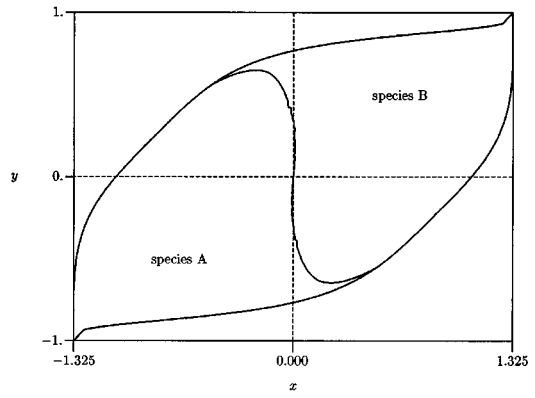

FIG. 5. Set of species defined for $\gamma=25$, $b=\Delta_x=1$.

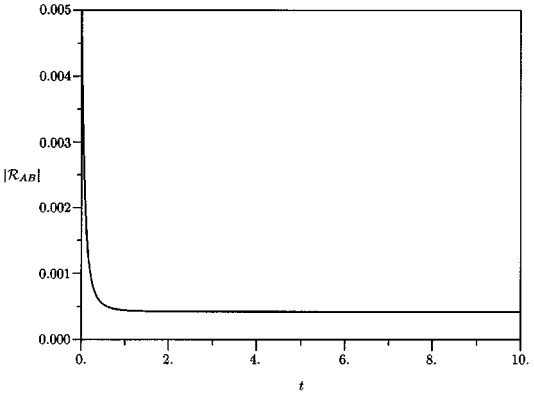

FIG. 6. Integrated memory function as a function of time obtained by direct simulation for $\gamma=25$, $b=\Delta_x=1$.

3. Characteristic function

For each type of simulation, the hardest task is to evaluate the characteristic functions, that is to determine if a given phase point is within a given species. A very general method that can be used to solve this problem is to count how many times a ray originating from the position of the realization in phase space intersects the species boundary. The realization is inside the species, if and only if, there is an odd number of intersections. In two dimensions, the boundary is most simply implemented as a sequence of segments. Even if the ray is arbitrary, the computations are much easier if it is parallel to one of the axes. We chose a ray that points toward the positive x axis. The execution time of the algorithm scales as the number of segments describing the boundary. In order to reduce the execution time, the species area is partitioned by equidistant lines parallel to the y axis. The computation is then executed in two steps. First, we determine in which strip, described by a small number of segments, the realization may be. Then, the algorithm described above is used to establish if it is there or not.

B. Results

In the case $b=\Delta_x=1$ and $\gamma=25$, the existence of a plateau for the function $\mathcal{R}_{AB}(t)$ ($\tau_{\text{mic}}\ll t\ll\tau_{\text{pop}}$) supports the validity of the phenomenological rate law (2.17) (Fig. 6). By symmetry, $\tau_{AA}^{-1}=|\tau_{AB}^{-1}|$ so that $\tau_{\text{pop}}^{-1}=2\tau_{AB}^{-1}$ [Eq. (2.21)]. Since the lifetime of the transients is of order τ_{mic}, we observe that $\tau_{\text{mic}}\sim 10^{-1}$ in this case. We also observe that $\tau_{\text{pop}}\sim 10^{3}$. This further confirms the separation of time scales and the validity of the phenomenological rate law for this case. The same conclusion is obtained when the results from a simple phenomenological simulation are fitted to Eq. (2.17) (Fig. 7). Transition rates obtained using both types of simulation are compiled in Table I. In all cases, η_α is numerically evaluated as being close to 0.5, as required by the symmetry of Eq. (2.1) when considering model (3.1).

We notice that the transition rates obtained using the two methods are of the same order of magnitude even though they differ by a factor of approximately 2. In particular, for the case where $b=\Delta_x=1$ (Fig. 8), direct simulations give

$$\tau_{\text{pop}}^{-1}=0.789\ \exp(-0.273\gamma)$$

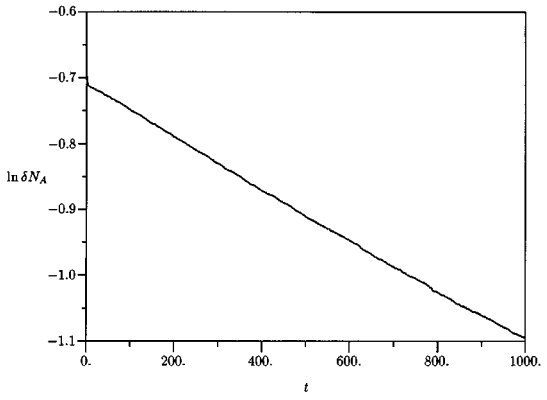

FIG. 7. Decay of the A-population number obtained by simple phenomenological simulation for $\gamma=25$, $b=\Delta_x=1$.

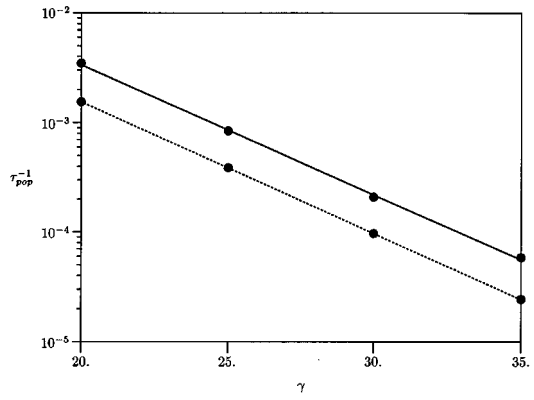

FIG. 8. Phenomenological transition rates for the bivariate system ($b=\Delta_x=1$). The continuous line corresponds to the direct simulation calculation, whereas the dotted one describes the phenomenological simulation. The statistical uncertainty is smaller or equal to the extent of the points.

and simple phenomenological simulations,

$$\tau_{\mathrm{pop}}^{-1}=0.394\ \exp(-0.277\gamma).$$

This result is encouraging considering the choice of finite elements, i.e., C^0 linear interpolation functions for $p_{\pm}^{s}(\vec{x})$. Since the vector fields $\vec{J}^{s}(\vec{x})$ and $\vec{K}^{s}(\vec{x})$ can be considered as derivatives of these distributions, this approximation is somewhat crude. Using higher-order interpolation functions providing C^1 continuity between elements would improve both the positioning of the interspecies boundary and the value of $\vec{\nabla}\cdot\vec{K}^{s}(\vec{x})$ in Eq. (2.20). The results of the direct simulation could therefore be improved quite a bit by such a modification. On the other hand, the results of the simple phenomenological simulations would probably be about the same as long as the boundary stays well within the region of low probability density separating the two peaks.

The results of the simple phenomenological simulations are very close to those obtained for the univariate system $\dot{x}=-x^3+bx\pm\Delta_x$ [17,18]. For this system, the interspecies boundary is given by the y axis. The probability in the region enclosed between this boundary and the bivariate interspecies one is small since the latter is located between the probability density peaks. Therefore, the two sets of species do not differ enough to be easily distinguishable using a simple phenomenological simulation. It demonstrates that the effect of the y variable is small in the present case.

V. CONCLUSION

The present study has investigated the usefulness of direct simulations to study multistable multivariate systems subjected to Markovian dichotomous noise. In the case of a bistable bivariate system, the existence of a regime in which the phenomenological rate law (2.17) is valid has been demonstrated using both direct simulations and simple phenomenological simulations. In doing so, we established a species definition criterion.

Direct simulations are an effective way to evaluate interspecies transition rates. However, they are very dependent on the positioning of the interspecies boundaries and on the value of the probability densities. Great care must therefore be taken in calculating them. In this respect, more work needs to be done to verify the validity of Eq. (2.20), particularly in using higher-order finite elements. These elements could also render useless the use of a smoothing procedure.

The speed of a simple phenomenological simulation is limited by the time required for a transition to occur. On the other hand, a direct simulation execution speed is limited by the subtraction $\langle\theta_{\beta}^{r}(\Delta t|\vec{x},-\vec{\Delta})\rangle-\langle\theta_{\beta}^{r}(\Delta t|\vec{x},+\vec{\Delta})\rangle$ found in Eq. (2.20). As this difference decreases, the number of samples generated needs to increase in order to obtain sufficient precision. Even with this limitation, direct simulations are a very powerful tool because of their capability of simultaneously determining transition rates that are of the same order of magnitude in multispecies systems.

Even if the bivariate system studied here is deterministically decoupled, the shape of the support is not trivial. Furthermore, the steady-state probability density shows a great deal of diversity as the parameters are varied. This clearly

TABLE I. Transition rates for the bivariate system (3.1) ($b=\Delta_x=1$). The uncertainties are determined using a linear regression to adjust the simulation results to Eqs. (2.17) and (2.20) and thus only represent statistical errors.

γ	η_A	τ_{pop}^{-1}	
		Direct simulation	Phenomenological simulation
20	0.4997	$(3.47\ \pm0.02)\times10^{-3}$	$(1.55\pm0.06)\times10^{-3}$
25	0.5001	$(8.44\ \pm0.02)\times10^{-4}$	$(3.9\ \pm0.1)\times10^{-4}$
30	0.5004	$(2.097\pm0.004)\times10^{-4}$	$(9.7\ \pm0.2)\times10^{-5}$
35	0.5024	$(5.84\ \pm0.02)\times10^{-5}$	$(2.44\pm0.07)\times10^{-5}$

illustrates the rich behavior that can arise from an apparently simple system when it is subjected to noise.

This tool should prove very useful in studying stochastic systems. One such bivariate system is the quartic potential coupled to the Morse oscillator [24]. This system is used in model isomerization reactions coupled to an internal rotational degree of freedom. In this case, the noise could represent the stochastic variations of an external electric field applied to the isomers. Furthermore, univariate inertial systems could be studied using the same approach by introducing a second variable representing velocity.

Some of the algorithms implemented here could be used to study systems described by more than two variables, while others would need to be redesigned. For instance, the finite elements and smoothing procedures could be generalized relatively straightforwardly to systems described by more variables. On the other hand, the meshing algorithm would require more modifications. Furthermore, the algorithms used to determine the support and the species boundaries depend to a large extent on the topology of the problem. Their generalization to other types of systems is possible, but would require further work. With respect to the simulations, the only element that would require some efforts is the evaluation of the characteristic function. Even if it can, in principle, be generalized to any number of variables, its generalization would require further work.

The theory presented here is not restricted to fixed points. It can equally well be applied to other types of attractors such as limit cycles. The algorithms presented here can easily be modified to consider such bivariate systems. Finally, the theory could be generalized to study systems subjected to multiplicative or asymmetric Markovian dichotomous noise.

ACKNOWLEDGMENTS

This research was supported by grants from the National Sciences and Engineering Research Council of Canada.

APPENDIX A: CHARACTERISTIC FUNCTION GRADIENT

We consider the integral Ψ:

$$\Psi = \int_{\Re^n} d^n x \; \vec{\nabla}\theta_\alpha(\vec{x}) \cdot \vec{A}(\vec{x}), \tag{A1}$$

where $\vec{A}(\vec{x})$ is an arbitrary vector function and $\theta_\alpha(\vec{x})$, the characteristic function (2.9). Clearly, $\vec{\nabla}\theta_\alpha(\vec{x})$ is zero everywhere except on the boundary $\partial\Omega_\alpha$, where $\theta_\alpha(\vec{x})$ is discontinuous. Since the exact value of $\theta_\alpha(\vec{x})$ on the boundary is not important for the following argument, it can be approximated by the function $\theta'_\alpha(\vec{x})$:

$$\theta'_\alpha(\vec{x}) \equiv \begin{cases} 1 & \text{if} \quad \vec{x} \in \Omega_\alpha, \quad \vec{x} \notin \partial\Omega_\alpha \\ \frac{1}{2} & \text{if} \quad \vec{x} \in \partial\Omega_\alpha \\ 0 & \text{otherwise.} \end{cases}$$

The discontinuity of the function $\theta'_\alpha(\vec{x})$ and the boundary's position can be described by

$$\theta'_\alpha(\vec{x}) = H(f(\vec{x}))$$

where $H(x)$ is the Heaviside step function:

$$H(x) \equiv \begin{cases} 0 & \text{if} \quad x<0 \\ \frac{1}{2} & \text{if} \quad x=0 \\ 1 & \text{if} \quad x>0 \end{cases}$$

and $f(\vec{x})$ is a continuous function such that

$$f(\vec{x}) \begin{cases} >0 & \text{if} \quad \vec{x} \in \Omega_\alpha, \quad \vec{x} \notin \partial\Omega_\alpha \\ =0 & \text{if} \quad \vec{x} \in \partial\Omega_\alpha \\ <0 & \text{otherwise.} \end{cases}$$

Equation (A1) can therefore be expressed as

$$\Psi = \int_{\Re^n} d^n x \; \vec{\nabla} f(\vec{x}) \cdot \vec{A}(\vec{x}) \, \delta(f(\vec{x})).$$

We partition the $\mathcal{R}^n$ space in disjoint regions Ω^k such that for each one of them we can choose a coordinate x^{ki} with respect to which $f(\vec{x})$ has only simple zeros. In other words, in each region Ω^k, $\partial_{x^{ki}} f(\vec{x}) \neq 0$ at each point where $f(\vec{x}) = 0$. The function $f(\vec{x})$ can then be taken out of the Dirac delta function:

$$\Psi = \sum_{jk} \int_{\Omega^k} d^n x \; \vec{\nabla} f(\vec{x}) \cdot \vec{A}(\vec{x}) \, \frac{\delta(x - x^{ki}_{0j})}{|\partial_{x^{ki}} f(x^{ki}_{0j})|}.$$

The sum over k is carried out over the regions Ω^k and the one over j, over the simple zeros x^{ki}_0 of $f(\vec{x})$ with respect to the coordinate x^{ki} inside the region Ω^k. By integrating within each region Ω^k over the coordinate x^{ki}, we get

$$\Psi = \sum_{jk} \int_{\Omega^k|_{f(\vec{x})=0}} d^{n-1} x \; \vec{\nabla} f(\vec{x}) \cdot \vec{A}(\vec{x}) \, \frac{1}{|\partial_{x^{ki}} f(x^{ki}_{0j})|},$$

where within each region Ω^k, the integral is carried out over the $n-1$ coordinates excluding x^{ki}, this last one being implicitly given by the equation $f(\vec{x}) = 0$.

At an arbitrary point $\vec{x}_0$ on the boundary $\partial\Omega_\alpha$, the unit vector $\hat{N}_{\partial\Omega_\alpha}$ perpendicular to $\partial\Omega_\alpha$ and pointing outside of Ω_α is given by

$$\hat{N}_{\partial\Omega_\alpha} = -\frac{\vec{\nabla} f(\vec{x}_0)}{|\vec{\nabla} f(\vec{x}_0)|}.$$

We therefore get

$$\Psi = -\sum_{jk} \int_{\Omega^k|_{f(\vec{x})=0}} d^{n-1} x \; \hat{N}_{\partial\Omega_\alpha} \cdot \vec{A}(\vec{x}) \left| \frac{\vec{\nabla} f(\vec{x}_0)}{\partial_{x^{ki}} f(x^{ki}_{0j})} \right|.$$

In order to evaluate this integral, we need to parametrize the boundary using an appropriate set of coordinate systems. With this in mind, we partition the boundary $\partial\Omega_\alpha$ into subboundaries $\partial\Omega^l_\alpha$ for each of which an $n-1$ dimensional coordinate system $\vec{x}'^{\,l}$ can be defined. The summation over j is

now unnecessary, being implicitly implemented by the transformation. The integral can be rewritten as

$$\Psi = -\sum_{kl} \int_{\partial\Omega_\alpha^l \cap \Omega^k} d^{n-1}x'^l \hat{N}_{\partial\Omega_\alpha} \cdot \vec{A}(\vec{x}'^l) \left| \frac{\vec{\nabla} f(\vec{x}_0)}{\partial_{x^{ki}} f(x_0^{ki})} \right| \frac{\partial_k(\vec{x})}{\partial(\vec{x}'^l)}, \tag{A2}$$

where $\partial_k(\vec{x})/\partial(\vec{x}')$ is the Jacobian of the transformation from the $n-1$ coordinates of $\vec{x}$ excluding x^{ki} to the coordinate system $\vec{x}'^l$. We define the quantity $g(\vec{x}'^l)$:

$$g(\vec{x}'^l) = \left| \frac{\vec{\nabla} f(\vec{x}_0)}{\partial_{x^{ki}} f(x_0^{ki})} \right| \frac{\partial_k(\vec{x})}{\partial(\vec{x}'^l)}, \quad \vec{x}'^l \in \partial\Omega_\alpha^l \cap \Omega^k, \tag{A3}$$

and denote the summation and integration procedure in Eq. (A2) by $\int_{\partial\Omega_\alpha} d^{n-1}x$. We can now write

$$\Psi = -\int_{\partial\Omega_\alpha} d^{n-1}x'^l g(\vec{x}'^l) \hat{N}_{\partial\Omega_\alpha} \cdot \vec{A}(\vec{x}'^l). \tag{A4}$$

In two-dimensional space, it is convenient to parametrize the boundary by its length because in that case $g(\vec{x}'^l)=1$.

APPENDIX B: HEISENBERG PROPAGATOR

This calculation is inspired from one found in [10]. Let $A(\vec{x},k\vec{\Delta})$ be a dynamical variable defined on the system's state $\vec{x}$ and the noise $k\vec{\Delta}$, where $k=\pm$. Its average at time t on a set of realizations and on the initial conditions can be calculated in two different but equivalent ways ($i=\pm$):

$$\langle A(\vec{x},k\vec{\Delta})\rangle_t = \sum_i \int_{\Re^n} d^n x \langle A^r(t_0|\vec{x},i\vec{\Delta},t_0)\rangle p_i(\vec{x},t) \tag{B1}$$

$$= \sum_i \int_{\Re^n} d^n x \; p_i(\vec{x},t_0) \langle A^r(t|\vec{x},i\vec{\Delta},t_0)\rangle, \tag{B2}$$

where $p_i(\vec{x},t)$ is defined as the probability that the system be in state $\vec{x}$ and that the noise be equal to $i\vec{\Delta}$ at time t, and $A^r(t|\vec{x},i\vec{\Delta},t_0)$, as the value of the dynamical variable A at time t for a given realization initiated at time t_0 with the system in state $\vec{x}$ and the noise equal to $i\vec{\Delta}$. The operator $\langle\cdots\rangle$ represents an average over realizations, and the operator $\langle\cdots\rangle_t$, an average carried out at time t over realizations and initial conditions.

In the first equation, it is the probability density that evolves over time, while in the second one, it is the dynamical variable's average. These two equations therefore correspond, respectively, to the Schrödinger and Heisenberg pictures. From Eq. (B1), we obtain

$$\langle A(\vec{x},k\vec{\Delta})\rangle_t = \sum_{ij} \int_{\Re^n} d^n x \langle A^r(t_0|\vec{x},i\vec{\Delta},t_0)\rangle (e^{\mathbf{D}t})_{ij} p_j(\vec{x},t_0)$$

$$= \sum_{ij} \int_{\Re^n} d^n x \; p_j(\vec{x},t_0) (e^{\mathbf{D}^\dagger t})_{ji} \langle A^r(t_0|\vec{x},i\vec{\Delta},t_0)\rangle, \tag{B3}$$

where $e^{\mathbf{D}t}$ is the propagator of $p_i(\vec{x},t)$, that is the Schrödinger propagator, and $\mathbf{D}^\dagger$, the operator adjoint to $\mathbf{D}$.

The initial probability densities being arbitrary, Eqs. (B2) and (B3) imply that $e^{\mathbf{D}^\dagger t}$ is the propagator of the average $\langle A^r(t|\vec{x},i\vec{\Delta},t_0)\rangle$:

$$\langle \mathbf{A}^r(t|\vec{x},t_0)\rangle = e^{\mathbf{D}^\dagger t} \langle \mathbf{A}^r(t_0|\vec{x},t_0)\rangle,$$

where

$$\mathbf{A}^r(t|\vec{x},t_0) = \begin{bmatrix} A^r(t|\vec{x},+\Delta,t_0) \\ A^r(t|\vec{x},-\Delta,t_0) \end{bmatrix}.$$

It now appears clearly that $\mathbf{D}^\dagger$ is the evolution operator of the average $\langle \mathbf{A}^r(t|\vec{x},t_0)\rangle$:

$$\frac{\partial}{\partial t} \langle \mathbf{A}^r(t|\vec{x},t_0)\rangle = \mathbf{D}^\dagger \langle \mathbf{A}^r(t|\vec{x},t_0)\rangle.$$

[1] C. M. Bowden, M. Clifton, and H. R. Robb, *Optical Bistability* (Plenum, New York, 1982).

[2] *Oscillations and Traveling Waves in Chemical Systems*, edited by R. Field and M. Burger (Wiley, New York, 1985).

[3] P. Gray and S. K. Scott, *Chemical Oscillations and Instabilities* (Oxford University Press, Oxford, 1990).

[4] A. T. Winfree, *The Geometry of Biological Time* (Springer, New York, 1980).

[5] W. Horsthemke and R. Lefever, *Noise-Induced Transitions: Theory and Applications in Physics, Chemistry, and Biology*, Springer Series in Synergetics Vol. 15 (Springer-Verlag, New York, 1984).

[6] *Noise in Nonlinear Dynamical Systems*, edited by F. Moss and P. McClintock (Cambridge University Press, Cambridge, 1988).

[7] I. L'Heureux, R. Kapral, and K. Bar-Eli, J. Chem. Phys. **91**, 4285 (1989).

[8] I. L'Heureux, Phys. Lett. A **171**, 204 (1992).

[9] I. L'Heureux and R. Kapral, J. Chem. Phys. **88**, 7468 (1988).

[10] B. J. Berne, in *Statistical Mechanics, Part B: Time-Dependent Processes*, edited by B. J. Berne (Plenum, New York, 1977), Chap. 5, pp. 233–257.

[11] D. Chandler, J. Chem. Phys. **68**, 2959 (1978).

[12] P. Grigolini, Phys. Lett. A **119**, 157 (1986).

[13] S. Faetti, L. Fronzoni, P. Grigolini, and R. Mannella, J. Stat. Phys. **52**, 951 (1988).

[14] S. Faetti, L. Fronzoni, P. Grigolini, V. Palleschi, and G. Tropiano, J. Stat. Phys. **52**, 979 (1988).

[15] M. Bianucci, R. Mannella, B. J. West, and P. Grigolini, Phys. Rev. E **51**, 3002 (1995).

[16] I. L'Heureux, Phys. Rev. E **51**, 2787 (1995).

[17] I. L'Heureux and R. Kapral, J. Chem. Phys. **90**, 2453 (1989).

[18] J. M. Porrà, J. Masoliver, K. Lindenberg, I. L'Heureux, and R. Kapral, Phys. Rev. A **45**, 6092 (1992).

[19] I. L'Heureux and R. Kapral, Phys. Lett. A **136**, 472 (1989).
[20] K. Kitahara, W. Horsthemke, and R. Lefever, Phys. Lett. A **70**, 377 (1979).
[21] J. M. Sancho and M. San Miguel, Prog. Theor. Phys. **69**, 1085 (1983).
[22] F. Sagués, M. San Miguel, and J. M. Sancho, Z. Phys. B **55**, 269 (1984).
[23] O. C. Zienkiewicz and K. Morgan, *Finite Elements and Approximation* (Wiley, Toronto, 1983); G. Dhatt and G. Touzot, *Une Présentation de la Méthode des Éléments Finis* (Les Presses de l'Université Laval, Québec, 1981); G. F. Carey and J. T. Oden, Vol. II of *The Texas Finite Element Series* (Prentice-Hall, Toronto, 1983).
[24] N. De Leon and B. J. Berne, J. Chem. Phys. **75**, 3495 (1981).